remote sensing

MDPI

Article

MODIS-Based Mapping of Secchi Disk Depth Using a Qualitative Algorithm in the Shallow Arabian Gulf

Muna. R. Al Kaabi *, Jun Zhao * and Hosni Ghedira

Department of Chemical and Environmental Engineering, Masdar Institute of Science and Technology, P.O. Box 54224, Masdar City, Abu Dhabi 54224, UAE; hghedira@masdar.ac.ae

* Correspondence: mralkaabi@masdar.ac.ae (M.R.A.K.); jzhao@masdar.ac.ae (J.Z.); Tel.: +971-2-810-9510 (J.Z.)

Academic Editors: Xiaofeng Li and Prasad S. Thenkabail
Received: 13 December 2015; Accepted: 5 May 2016; Published: 17 May 2016

Abstract: Regionally calibrated algorithms for water quality are strongly needed, especially for optically complex waters such as coastal areas in the Arabian Gulf. In this study, a regional qualitative algorithm was proposed to retrieve seawater transparency, with Secchi disk depth (SDD) as a surrogate, in the Arabian Gulf. A two-step process was carried out, first estimating the diffuse attenuation coefficient of downwelling irradiance at 490 nm (K_d_490) from MODIS/Aqua imagery and then SDD based on empirical correlations with K_d_490. Three satellite derived K_d products were tested and assessed against a set of *in situ* measurements, and one from a semi-analytical algorithm based on inherent optical properties gave the best performance with a R^2 of 0.62. Comparisons between the performances of SDD models developed in this study and those established in other regions indicated higher accuracy of our proposed model for the Gulf region. The potential factors causing uncertainties of the proposed algorithm were also discussed. Seasonal and inter-annual variations of SDD over the entire Gulf were demonstrated using a 14-year time series of MODIS/Aqua data from 2002 to 2015. High SDD values were generally observed in summer while low values were found in winter. Inter-annual variations of SDD did not shown any significant trend with exceptions during algal bloom outbreaks that resulted in low SDD.

Keywords: Arabian Gulf; water transparency; MODIS; Secchi disk depth; diffuse attenuation coefficient

1. Introduction

Water transparency is considered one of the key indicators for water quality assessment [1]. It has also been used as an easily measured proxy to describe the quantity of light availability in the aquatic environment [2]. Through measuring the degree of attenuation of sunlight that is caused by both scattering and absorption of all optically active components, *i.e.*, pure water, suspended sediment, colored dissolved organic matter (CDOM), and phytoplankton, water transparency provides information on incident sunlight penetration depth through the water column [3–7]. Although more sophisticated instruments are commercially available, Secchi disks are still being widely and regularly utilized to measure water transparency for oceanography and limnology. Secchi disk depth (SDD) is a relative indicator of the vertical visual clarity of light and also an indicator of trophic level [8–11].

Based on the contrast transmittance theory developed by Duntley [12] and Preisendorfer [13], many studies generally represent SDD as a hybrid function of optical properties, *i.e.*, the sum of the beam attenuation coefficient (c) and the diffuse attenuation coefficient of downwelling irradiance (K_d), within the visible spectrum [14,15]. However, numerous studies demonstrated that SDD is K_d-dependent rather than c-dependent [8,15,16]. Lee *et al.* [17] proposed a new theoretical model to interpret SDD, which relies only on K_d, unlike the classical model. They validated their model with measurements from different types of water and verified the high accuracy of the new model.

Compared with conventional field-based methods to measure water transparency, satellite remote sensing can provide synoptic views of the marine environment over large temporal and spatial scales. One of these satellite instruments, the Moderate Resolution Imaging Spectroradiometer (MODIS) instrument onboard the NASA Terra and Aqua satellites, provides daily global coverage at medium spatial resolution (250 m to 1000 m), and is an excellent candidate to map coastal water transparency on a daily basis. MODIS data have been successfully used for monitoring SDD or turbidity in different water bodies. Koponen *et al.* [18] used MODIS data to monitor turbidity in Finnish Lakes. A study was conducted in the Tampa Bay, Florida to monitor SDD using satellite measured K_d in the open water estuary using Sea-viewing Wide Field-of-View Sensor (SeaWiFS) satellite imagery [19]. In this study, a new approach was proposed to investigate the seasonality of SDD over four different parts of the Tampa Bay. Moreno *et al.* [20] used the reflectance at 645 nm (band 1) of MODIS/Terra to estimate turbidity and studied the effect of rainfall on turbidity. Wang *et al.* [21] established an algorithm to obtain turbidity from MODIS/Aqua derived normalized water-leaving radiance at the near-infrared band in Lake Okeechobee and Caloosahatchee and St. Lucie estuaries. They found seasonal, spatial, and event driven trends of turbidity in their study area, which were influenced by wind waves, hurricanes, and tides. More recently, Nehorai *et al.* [22] characterized the seasonal cycle of turbidity and plume spreading produced by flood events in the Dead Sea using MODIS imagery.

To the best of our knowledge, there are only three papers published about the water transparency in the Arabian Gulf (hereafter referred to as the Gulf) (Figure 1) although there are several papers addressing water quality variables. Al-Saadi *et al.* [23] investigated the water transparency from their field survey in the Shatt Al-Arab region in the northwestern Gulf. Alsahli *et al.* [24] developed a water clarity model using SeaWiFS and MODIS data for the Kuwait coastal waters. Al Kaabi *et al.* [25] established a regional algorithm to retrieve water turbidity in the coastal waters along the Abu Dhabi coast. However, seasonal and inter-annual variations in water transparency and their driving forces are still unknown. On the other hand, most of the published algorithms obtained transparency from radiance or reflectance [1]. When these algorithms are applied to satellite imagery, they may suffer from uncertainties over coastal and estuarine waters due to non-zero reflectance in the near-infrared (NIR) in turbid zones, and/or due to high loads of blue-absorbing aerosols in the atmosphere [26].

A semi-analytical algorithm developed by Lee *et al.* [27] has been validated to be accurate for estimates of the light attenuation coefficient [28]. In this study, a locally-adapted algorithm is developed to retrieve water transparency, with SDD as a proxy, from satellite derived K_d over the Gulf based on the Lee algorithm. The performance of the proposed algorithm is compared with those developed for other regions around the world. Using the regional SDD algorithm, seasonal and inter-annual variations of SDD from satellite measurements over the entire Gulf were examined and the driving forces were analyzed.

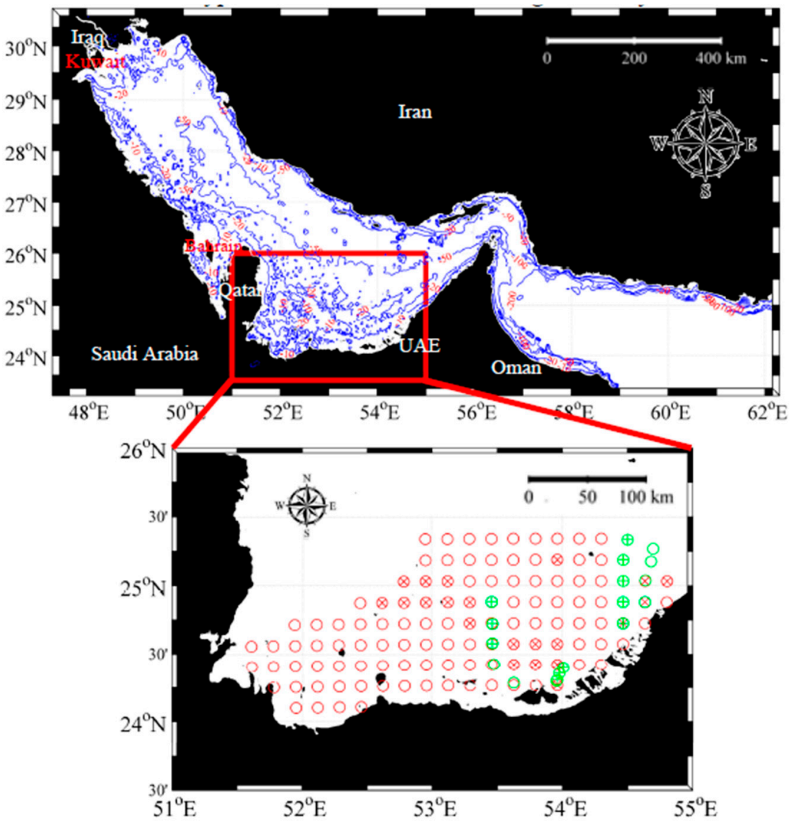

Figure 1. The upper panel shows a map of the Arabian Gulf with surrounding countries annotated. The isobaths of 10, 20, 50, 100, and 200 m are annotated. The bathymetry data are from NOAA with a spatial resolution of ~2 km. Sampling stations along the Abu Dhabi coast are shown in open circles. The red and green circles denote *in situ* measurements conducted by the Environmental Agency of Abu Dhabi (EAD) and the Masdar Institute of Science and Technology (MIST), respectively. The '×' and '+' indicate stations with matched satellite and *in situ* data measured by EAD and MIST, respectively.

2. Data and Methodology

2.1. Study Area

The Gulf is a semi-enclosed marginal sea about 1000 km long and about 200–300 km wide with an average depth of 35 m. The freshwater inflows into the Gulf are mainly located in the north and northwest [29]. For example, the Shatt al-Arab River discharges into the Gulf along the borders between Iran and Iraq. However, this freshwater input has reduced dramatically from the late nineties due to the draining of most of the Iraqi marshlands and the building of dams on Euphrates, Tigris and Karum rivers [30]. These conditions produce relatively low CDOM concentrations in the region (Al Shehhi *et al.*, in preparation). The salinity in the Gulf waters is high exceeding 40 psu (practical salinity units) and the water temperature can reach up to 34 °C during summer due to the arid climate. Despite these extreme conditions, coral reefs and benthic vegetation are found in the Gulf, as well as some endemic marine life, such as sea turtle, dugong, and dolphin, which highlights the importance of regular water quality monitoring.

The Gulf is subject to wind-driven and thermohaline dynamics due to its shallow nature. In the northern Gulf, predominant northwesterly wind, called Shamal, throughout the year, sets up coastal current regimes along both the Saudi (downwelling) and Iranian (upwelling) coasts [31]. In the southern region of the Gulf, the circulation is dominated by a counter-clockwise gyre in the surface. The water remains in the Gulf for about three to five years and leaves later through the Strait of Hormuz [32]. The Gulf atmosphere has high loads of dust, which results in high levels of dust

deposition as high as 30 $g \cdot m^{-2}$ [33]. Chlorophyll-a concentration in the Gulf waters is generally <1 $mg \cdot m^{-3}$ throughout all seasons with exceptions during bloom conditions when chlorophyll-a can be higher than 10 $mg \cdot m^{-3}$ [34]. In this regard, the transparency in the Gulf waters could be mainly caused by suspended sediments, which are of different origins, such as resuspension and deposition, given the relatively low concentrations of chlorophyll-a and CDOM [34]. Shamal winds as well as the intensive daytime summer winds that resulted from temperature differences between water and close landmass result in the increase in water density and wave actions, which leads to sinking of the surface water. The sinking of the surface water influences the coastal waters along the Emirates and made it vertically well-mixed and turbid [32].

The Abu Dhabi coast was chosen as a case study based on the following reasons. The UAE is one of the Gulf countries with arid to semi-arid climate due to scarcity of rainfall, high evaporation rate, and limited sources of freshwater. Underground and desalinated waters are the main source of potable water in the UAE, with the latter as the main source for domestic use. In fact, the UAE is the country with the second largest desalinating capacity, amounting to 14% of the total in the world [35]. The UAE coastal coral reef and sea grass ecosystems are threatened by several environmental hazards. For example, between August 2008 and August 2009, an extensive algal bloom outbreak in the Gulf was dominated by *Cochlodinium polykrikoides*, a toxin-producing species [36–38]. A large number of desalination plants in the UAE were forced to shut down, which caused a 40% decrease in freshwater production capacity. Another threat to Gulf water quality is oil spills that could have a dramatic impact on the local marine environment. The Gulf basin, surrounded by eight countries (*i.e.*, Bahrain, Iran, Iraq, Kuwait, Qatar, Saudi Arabia, and the UAE), is the most active oil production and trade area in the world. Frequent oil spill events have been reported in areas surrounding the UAE coast [39,40].

2.2. In Situ *Data Collection*

A Secchi disk with a diameter of 20 cm that had alternating black and white quadrants was used for SDD measurements. It had a weight at its base. A tape measure was used for SDD reading. Bottom depth was recorded by a sonar system on the research vessel. SDD collected from 139 stations along the Abu Dhabi coast (Figure 1) were used in this study. The maritime monitoring team of the Environment Agency of Abu Dhabi (EAD) collected 117 out of the 139 measurements over a three-month period from February to April 2010. The remaining 22 measurements were collected by the Coastal and Environmental Remote Sensing and Modeling laboratory at Masdar Institute of Science and Technology (MIST) from June 2013 to April 2014. For details regarding our filed campaigns, please refer to Mezhoud *et al.* [34].

A spectrometer (Ocean Optics USB2000+) was used to collect remote sensing reflectance (R_{rs}) following the NASA ocean optics data collection protocol [41]. Details regarding data collection and processing can be referred to Mezhoud *et al.* [34] and Zhao *et al.* [42]. R_{rs} data were obtained for 53 stations as displayed in Figure 1 in Mezhoud *et al.* [34].

2.3. Background for Existing K_d Algorithms

In this paper, three algorithms for K_d, two empirical and one semi-analytical, were tested to estimate SDD over the Gulf region. K_d expresses how light attenuates against depth. The relationship between K_d and SDD has been proven by previous studies [16,43,44].

SDD is predicted using satellite-derived K_d_490 from the empirical Mueller [45] and Morel [46] algorithms and the semi-analytical Lee algorithm [27]. The default K_d algorithm (Mueller) in SeaDAS correlated the blue-green band ratio of remote sensing reflectance R_{rs} with ground truth K_d data. The Mueller algorithm is expressed as:

$$K_d\_490\_mueller = 0.0166 + 10^{-0.8813 - 2.0584 \times x + 2.5878 \times x^2 - 3.4885 \times x^3 - 1.5061 \times x^4} \quad (1)$$

where x = log10(R_{rs}_488/R_{rs}_547).

Another empirical algorithm, developed by Morel [46,47], relates K_d to chlorophyll-a concentration (Chl) using different sets of *in situ* measurements:

$$K_d(\lambda) = K_w(\lambda) + x(\lambda)Chl^{e(\lambda)} \quad (2)$$

where $K_w(\lambda)$, $x(\lambda)$, and $e(\lambda)$ are empirical constants equal to 0.0166 m^{-1}, 0.07242, and 0.68955, respectively, at the wavelength of 490 nm [23]. Chl was derived from the operational band ratio algorithm. Then, Equation (2) can be rewritten as

$$K_d\_490\_morel = 0.0166 + 0.07242Chl^{0.68955} \quad (3)$$

However, these empirical algorithms usually fail when applied in optically complex coastal waters. They were generally designed for Case I waters, where phytoplankton dominates the light attenuation and other optically significant components co-vary with phytoplankton, which is not the same case for Case II waters. Lee *et al.* [27] developed a semi-analytical algorithm to estimate K_d_490 that works well for both deep and coastal waters with K_d_490 ranging from ~0.04 to 4 m^{-1}. This algorithm is expressed as:

$$K_d\_490\_lee = (1 + 0.005\theta_0)a(490) + 4.18(1 - 0.52e^{-10.8a(490)})b_b(490) \quad (4)$$

where a and b_b are the total absorption and backscattering of optically active constituents, and θ_0 is the solar zenith angle. This semi-analytical algorithm accounts for variations of inherent optical properties (IOPs) that determine apparent optical properties (AOPs) one of which is R_{rs} used in the empirical algorithms. Furthermore, the absorption and backscattering coefficients were derived from a quasi-analytical algorithm (QAA) that has been validated to be reliable and accurate for both Case I and Case II waters [27]. It should be noted that QAA is a model and needs region-dependent inputs, especially for case II waters, such as the spectral slope of detritus and CDOM absorption.

2.4. Satellite Image Processing and Matchup between Satellite and in Situ Measurements

MODIS Aqua level 0 (L0) data with a spatial resolution of 1 km corresponding to the dates when field surveys were carried out were downloaded from NASA ocean color data archive. L2 products, including K_d_490, K_d_488, and $K_d\_490\_morel$, were generated using the SeaDAS (Version 7.1) software package developed by NASA Ocean Biology Processing Group (OBPG). The default black pixel algorithm was used to carry out the atmospheric correction. The algorithm assumed that water-leaving radiance at the near-infrared (NIR) wavelengths is zero [48,49]. All products were projected with a cylindrical projection method.

We followed the NASA ocean optics protocol for the matchup analysis between *in situ* and satellite measurements [50]. The method is briefly described here. Satellite data of poor quality were discarded upon failure of any of the following tests: clouds, stray light, atmospheric correction failure, high top-of-atmosphere radiance, low water-leaving radiance, large solar/viewing angles, and navigation failure. With the stray light flag, pixels within 5 km distance to the land were not considered. Therefore, the tide-driven difference between satellite measurements and *in situ* observations can be ignored. Moreover, the tide in the Gulf region is small [51]. To allow for sufficient number of matchup for statistical analysis, a time window of 6 h between *in situ* and satellite measurements was adopted. Satellite data were extracted from a spatial window of 3 × 3 and the following criteria were implemented: (1) at least five out of the nine pixels have valid values and (2) the coefficient of variance (CV) calculated from the standard deviation divided by the mean is <40%. The matchup procedure resulted in 36 pairs of *in situ* SDD and satellite-derived K_d (out of the initial 139 measurements). Twelve pairs of *in situ* and satellite-derived R_{rs} were obtained and the stations with matched satellite and *in situ* measurements were L1, R1–R8, and R2.1–R4.1 (Please refer to Mezhoud *et al.* [34] for details). Satellite imagery corresponding to the time when field measurements for these stations were conducted was processed again using the short-wave infrared (SWIR) atmospheric correction scheme [52].

With the proposed algorithm for SDD (Section 4.2), monthly mean SDD from July 2002 to February 2015 over the whole Gulf (bounded by 23.2°–30.7°N and 47.3°–56.5°E) was calculated using the 4-km monthly K_d products based on the semi-analytical algorithm from NASA ocean color data archive. The climatology of monthly mean SDD was calculated from the multi-year monthly mean data. Seasonal SDD maps were then generated.

2.5. Statistical Analysis

In order to assess the performance of different algorithms in deriving SDD from satellite measured K_d, the following statistical indicators were used: determination coefficient (R^2), mean ratio, root mean square difference (RMSD), and relative percentage difference (RPD) between measured and estimated SDD, which are defined as follows:

$$\mathrm{RMSD} = \sqrt{\frac{\sum_{i=1}^{n}\left(\frac{\mathrm{SDD_{est(i)}}-\mathrm{SDD_{obs(i)}}}{\mathrm{SDD_{obs(i)}}}\right)^2}{n}} \times 100 \quad (5)$$

$$\mathrm{RPD} = \frac{\sum_{i=1}^{n}\frac{\mathrm{SDD_{est(i)}}-\mathrm{SDD_{obs(i)}}}{\mathrm{SDD_{obs(i)}}}}{n} \times 100 \quad (6)$$

where $\mathrm{SDD_{est}}$ and $\mathrm{SDD_{obs}}$ denote estimated and observed SDD, respectively.

3. Results

3.1. In Situ *Measured SDD*

The histogram of *in situ* measured SDD is shown in Figure 2. SDD varied between 1.68 and 16 m during the observation period on the west shelf of Abu Dhabi. The average of SDD was 7.33 m with a standard deviation of 2.47 m. Fifty-one out of the total 139 SDD observations ranged between 6 and 8 m. Twenty-four and 27 data points were located in the range of 4–6 m and 8–10 m, respectively. The lowest SDD was found in shallow coastal waters and the highest SDD was found in the offshore waters. As expected, SDD values showed an increasing trend towards offshore waters. In terms of seasonal variations, SDD indicated higher values in summer than in winter.

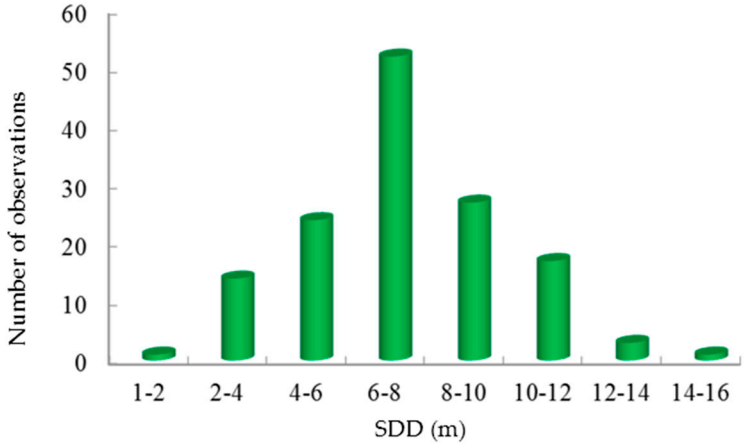

Figure 2. Histogram of *in situ* measured Secchi disk depth (SDD).

3.2. Development of New Models to Retrieve SDD from Satellite Derived K_d

As shown in Figure 3, reciprocals of satellite measured K_d_488_lee, K_d_490_morel and K_d_490_mueller are plotted against *in situ* measured SDD. Initial regression analysis indicated that the

relationships can be best fitted with quadratic functions. The best-fitted regression equations between satellite-derived $1/K_d$ and *in situ* measured SDD are list as follows:

$$SDD = 0.76 \times 1/K_d\_490\_mueller + 0.0018 \quad (7)$$

$$SDD = 0.93 \times 1/K_d\_490\_morel - 3.07 \quad (8)$$

$$SDD = 0.9 \times 1/K_d\_488\_lee + 1.01 \quad (9)$$

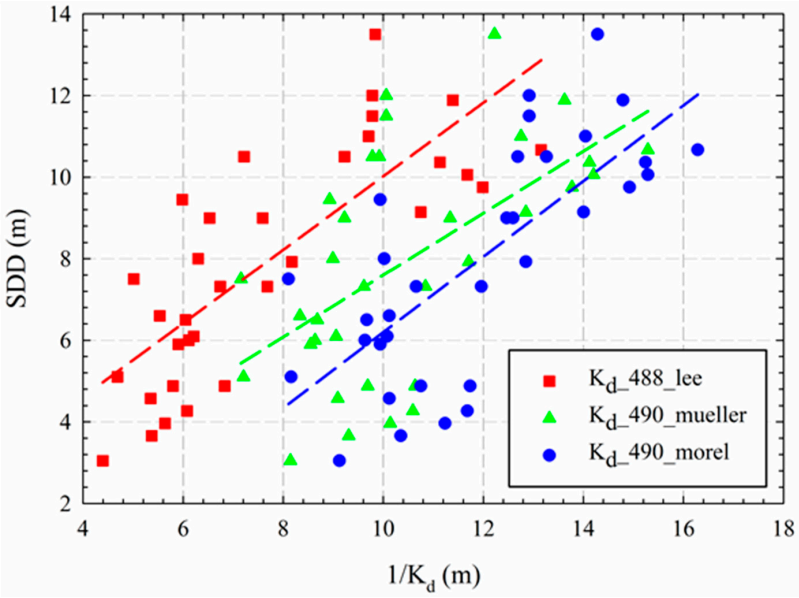

Figure 3. Relationships between *in situ* measured SDD and satellite-derived K_d_488_lee (solid red square), K_d_490_mueller (solid green triangle) and K_d_490_morel (solid blue circle). The red, green, and blue dashed lines denote the best fits between SDD and K_d_488_lee, K_d_490_mueller, and K_d_490_morel, respectively.

Statistical results for the relationships are summarized in Table 1. The highest R^2 of 0.6 was obtained with K_d_488_lee. The mean ratio between estimated and measured SDD is 1.06 for K_d_488_lee while 1.08 and 1.11 were obtained for K_d from Morel and Mueller algorithms, respectively. Overall, SDD was overestimated with K_d from Morel and Mueller algorithms. The highest RMSD of 40.82% was observed with K_d_490_mueller. The lowest RMSD of 26.68% was reached with K_d_488_lee. The lowest RPD (5.86%) was also obtained with K_d_488_lee. K_d from Morel and Mueller algorithms gave an RPD of 8.14% and 11.02%, respectively. Therefore, it can be concluded that K_d_488_lee outperformed K_d from Morel and Mueller algorithms in SDD retrieval. Hereafter, SDD based on the K_d_490_lee will be used for further analysis.

Table 1. Uncertainties of SDD from three models using different satellite derived K_d_490 as gauged by *in situ* measured SDD.

SDD Equation	R^2	Mean Ratio	RMSD (%)	RPD (%)
SDD = 0.9 × 1/K_d_488_lee + 1.01	0.62	1.06	26.68	5.86
SDD = 0.93 × 1/K_d_490_morel − 3.07	0.33	1.08	34.00	8.14
SDD = 0.76 × 1/K_d_490_mueller + 0.0018	0.52	1.11	40.82	11.02

To further compare the performance of the three tested algorithms, SDD maps have been generated for two days with contrasted optical properties (1 June 2004 and 23 December 2008). The produced

maps are presented in Figure 4. In the summer scene, high SDD values were observed when chlorophyll-a is low [53]. The spatial patterns of SDD from the three algorithms were similar. SDD estimated from the Mueller algorithm was lower than from the other two algorithms. Examination of K_d maps for 1 June 2004 (data not shown) demonstrated that K_d is generally <0.2 m^{-1} in the Gulf region. For this range of K_d, the Morel and the Mueller algorithms work well [41]. K_d_488_lee showed wide applicability for both coastal and oceanic waters for K_d values ranging from 0.04 to 4 m^{-1}. In contrast, in the winter scene, low SDD values were observed for high chlorophyll-a concentrations. A major red tide outbreak was recorded in December 2008 [37]. In the bloom affected areas to the south of Iran, both K_d_490_mueller and K_d_488_lee produced low SDD values <1 m while SDD from K_d_490_morel led to higher SDD values >4 m. On the other hand, both K_d_490_morel and K_d_490_mueller produced lower SDD values than those obtained by K_d_488_lee in the southern Gulf region while the K_d_490_mueller showed higher SDD values than the other two algorithms in the northern Gulf region.

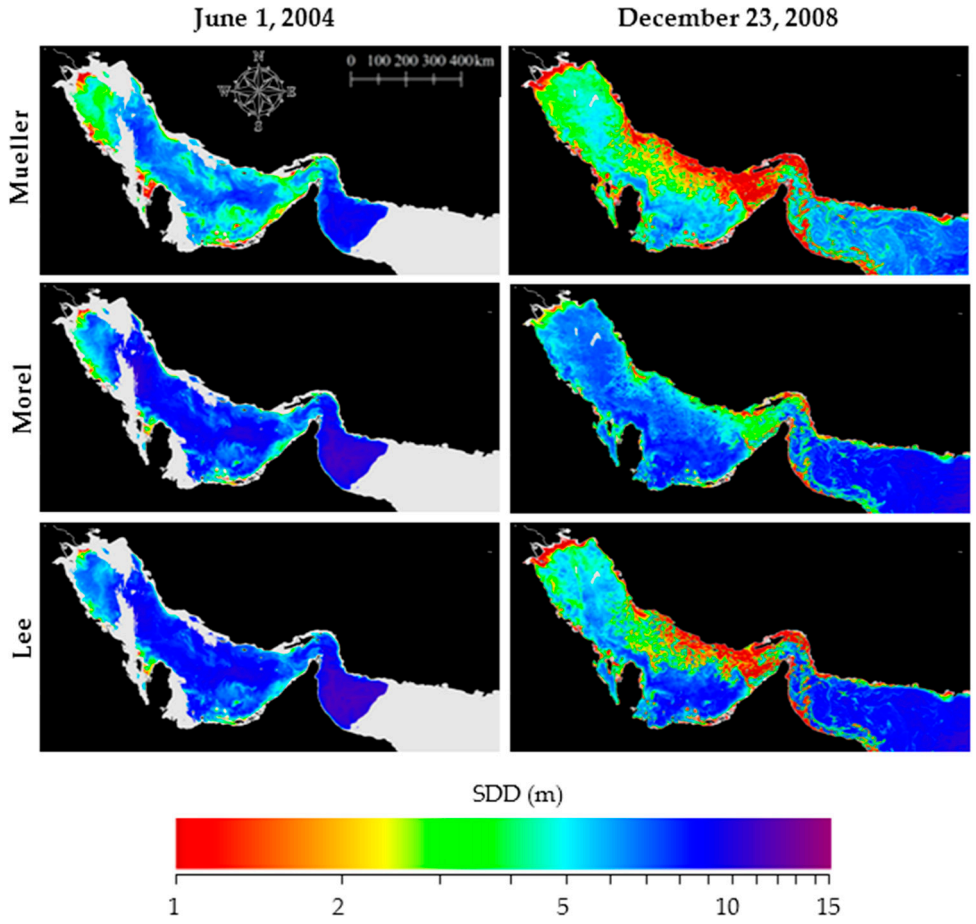

Figure 4. Examples of SDD maps generated based on Aqua derived K_d_490_mueller, K_d_490_morel, and K_d_488_lee. The two-day scenes from summer and winter, respectively, were chosen randomly. The dates are annotated. The top, middle and bottom panels represent SDD maps from K_d using the Mueller, Morel, and Lee algorithms, respectively.

4. Discussion

4.1. Comparison with Other Models

Different models to retrieve SDD have been proposed in different regions around the world. Chen *et al.* [26] developed an empirical SDD algorithm in the Tampa Bay, Florida and examined the

spatial and temporal variability of water transparency using SeaWiFS-derived SDD. Pierson *et al.* [54] studied the relationship between K_d_490 and SDD using their field measurements in the Baltic Sea and suggested that the relationship was useful for application of satellite remote sensing. Based on *in situ* measurements, Suresh *et al.* [55] proposed an empirical algorithm to obtain SDD from K_d_490 along the west coast of India in the Arabian Sea. The performances of these published algorithms were assessed and compared with that of the algorithm proposed over the Gulf region in this study. The field measured SDD is plotted against estimated SDD in Figure 5. Data points from our proposed algorithm (Equation (9)) lie close to the 1:1 line while those from others overestimate [54,55] or underestimate [26].

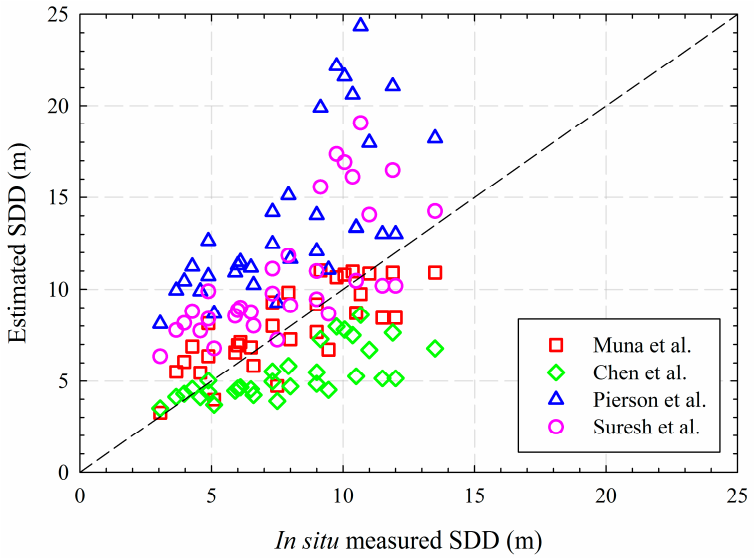

Figure 5. Comparison between the model proposed in our study and those published in the literature as gauged by *in situ* measured SDD. The dashed line represents the 1:1 relationship.

The statistical results are shown in Table 2. SDD estimated from our developed algorithm showed the best agreement with *in situ* measurements with a R^2 of 0.6. Compared with other models, the algorithm proposed in this study had a mean ratio closest to 1, nominally 1.06. The best performance of our developed algorithm is also proven by the smallest RMSD and RPD of 26.68% and 5.86%, respectively. With respect to the slope and intercept from the linear regression between measured and estimated SDD, Pierson *et al.*'s model [54] produced a slope of 1.08 while the largest intercept of 5.27 compared with results using other models. Although the Suresh *et al.*'s model [55] performed better than ours in terms of slope, the RMSD and RPD from their model are over twice and seven times, respectively, larger than from our model. Therefore, it can be concluded that the models proposed for other regions are not suitable for our study area. The reason of this lower performance is mainly due to the unique optical properties of the Gulf waters. For example, the water column in the Tampa Bay has a high content of CDOM, which is not the same case as in the Gulf. Region-specific algorithms for satellite-based transparency retrievals are indeed highly recommended.

Table 2. Uncertainties of SDD from different models as gauged by *in situ* measured SDD.

Model	R^2	Mean Ratio	RMSD (%)	RPD (%)	Slope	Intercept
This study (Equation (9))	0.6	1.06	26.68	5.86	0.6	3.17
Chen *et al.* (2007) [26]	0.48	0.73	33.51	−27.07	0.34	2.65
Pierson *et al.* (2008) [54]	0.47	1.85	97.25	84.64	1.08	5.27
Suresh *et al.* (2006) [55]	0.47	1.44	58.12	44.42	0.84	4.12

4.2. Potential Factors Causing Uncertainties of the Algorithm

This section addresses the potential factors that produce uncertainties of the proposed algorithm in this study. It should be noted that the effects of the factors on the performance of the algorithm is demonstrated in a qualitative way.

As stated above, K_d_488_lee gave the highest performance in deriving SDD in the Gulf. This finding could be explained by the following:

(1) The Lee algorithm takes into consideration both absorption and scattering of all optically active components while the Mueller and Morel algorithms are more sensitive to the changes in water absorption [56].

(2) The empirical algorithms are designed for case I waters where CDOM and non-algal particulate co-vary with phytoplankton. Most of these algorithms have failed when applied in turbid case II waters [57,58]. Furthermore, the default parameters used by these algorithms were proposed for global scale applications. For local and regional studies, those parameters must be re-calibrated with new sets of locally collected measurements to improve the performance of these empirical algorithms.

However, uncertainties still exist with respect to the Lee algorithm. This semi-analytical algorithm was originally designed for optically deep waters [27]. Thus, its performance would be affected when used in areas affected by bottom reflection [28]. Barnes *et al.* [59] found that the standard Lee algorithm overestimated the true K_d_488 by a factor of 2 or above in the Florida Reef Tract region. They modified the semi-analytical algorithm to remove bottom contamination to improve the K_d retrieval accuracy from MODIS measurements over the optically shallow waters in the Florida Keys. This modified version was successfully validated against a set of *in situ* measurements. For data points used for the algorithm development in this study, only those from stations with bottom depth >10 m that meets requirements of "optically deep waters" as per Cannizzaro *et al.* [60] using our field measured R_{rs} were considered. Therefore, bottom reflection will not affect the algorithm developed to compute SDD. What will compromise the performance of the algorithm is satellite-derived K_d itself. For example, satellite-derived K_d is not realistic for those clear shallow waters, such as along the east coast of Qatar where bottom depth is <10 m.

Satellite-based techniques for water transparency mapping require clear sky conditions. Satellite images used in this study went through a comprehensive atmospheric correction procedure. The operational atmospheric correction scheme assumes that the water-leaving radiance in the near infrared (NIR) region is insignificant and can be neglected. However, this assumption is gradually compromised as the transparency increases, especially for optically complex coastal waters. Different algorithms have been developed for turbid coastal and inland waters. Wang and Shi [52] proposed an approach using the combined near-infrared (NIR) and shortwave infrared (SWIR) bands for MODIS/Aqua. Their algorithm has been tested and evaluated in different turbid waters, such as Taihu Lake, Eastern China Seas, and showed positive results [61–63]. The SWIR algorithm has been integrated into the SeaDAS package. In this study, we compared the results by implementing the default and SWIR atmospheric correction schemes. Figure 6 shows the comparisons between *in situ* and satellite-derived R_{rs} for bands centered 412, 443, 488, 547, and 667 nm that are involved during the QAA algorithm implementation. The statistical results are listed in Tables 3 and 4. It can be seen that (1) both the default and SWIR algorithms underestimated R_{rs}; (2) satellite-derived measurements were in good agreement with *in situ* observations, as indicated by the high R^2, mean ratio and slope close to 1, and low RMSD, except for 412 and 667 nm. This could be related to the relatively low values at these two bands. It should be noted that dust has significant effects on satellite measurements in the ultraviolet region [64]. Therefore, the relatively low accuracy of R_{rs} at 412 nm can also be associated with the high loading of dust in the atmosphere over the study area; (3) The performances of the two algorithms are similar. There is no significant improvement by implementing the SWIR algorithm over our study area. Although various approaches were proposed to correct atmospheric

dust aerosols [65–67], no operational atmospheric correction scheme for dust correction of ocean color data is available. In SeaDAS processing from level 1 to level 2, the default thresholds of cloud albedo and aerosol optical depth at 865 nm (AOD_865) are 0.027 and 0.3, respectively. Pixels with cloud albedo and AOD_865 larger than the thresholds will be masked. Although relaxation of these criteria was tested by Doxaran *et al.* [68] with careful visual check of the produced results, operational implementation of the approach with quality assured products is impossible. Therefore, regional specific atmospheric correction schemes would be required to improve the accuracy of application of ocean color data over the Gulf region with relatively high loads of airborne dust. With aim to monitor transparency with large spatial and temporal coverage, using satellite data without correcting aerosol contributions may be an alternative to circumvent the difficulties with respect to the atmospheric correction, such as the approach proposed by Qiu *et al.* [69].

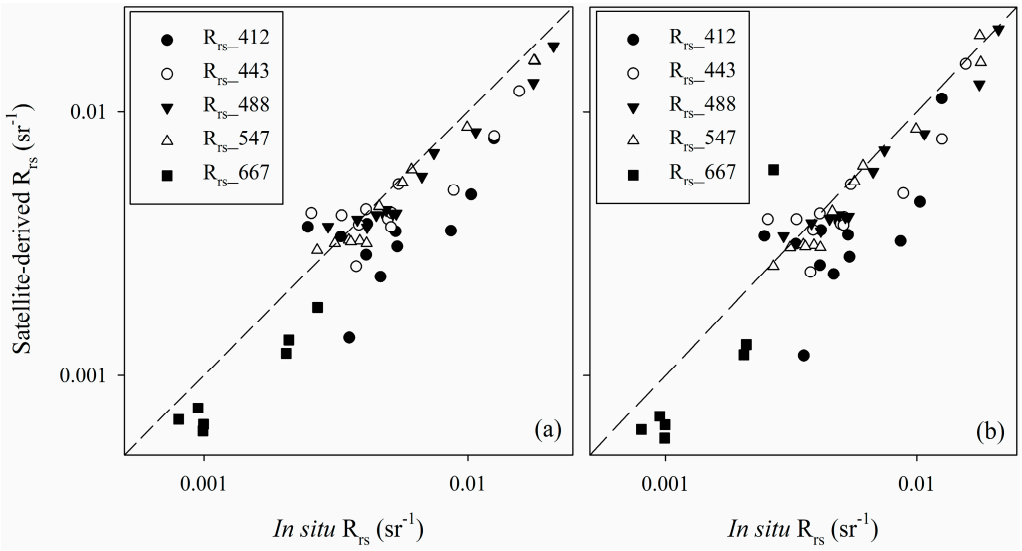

Figure 6. Comparisons between Aqua-derived and *in situ* measured R_{rs} for bands centered at 412, 443, 488, 547, and 667 nm. These bands were involved in the QAA algorithm implementation. The default (**a**) and SWIR (**b**) atmospheric correction schemes were carried out.

Table 3. Comparison between *in situ* and satellite-derived R_{rs} using the default atmospheric correction method.

Model	R^2	Mean Ratio	RMSD (%)	RPD (%)	Slope	Intercept
412	0.62	0.71	17.04	−28.66	0.4	0.0014
443	0.87	0.9	8.87	−10.09	0.59	0.0014
488	0.98	0.88	3.12	−11.57	0.76	0.0007
547	1	0.92	1.37	−7.91	0.86	0.0003
667	0.89	0.6	17.49	−39.69	0.67	0.00008

Table 4. Comparison between *in situ* and satellite-derived R_{rs} using the SWIR atmospheric correction method.

Model	R^2	Mean Ratio	RMSD (%)	RPD (%)	Slope	Intercept
412	0.62	0.69	17.33	−30.52	0.63	0.0002
443	0.82	0.89	8.07	−10.96	0.76	0.0004
488	0.95	0.88	2.92	−12.28	0.86	0.00005
547	0.97	0.91	1.67	−8.86	0.99	0.0004
667	0.66	0.7	32.41	−30.2	2.06	−0.0016

SDD values used for algorithm development varied between 1.68 and 16 m, which corresponded to chlorophyll-a concentrations in the range of 0.08–3.9 mg·m^{-3} [34]. The Gulf is subject to frequent algal bloom outbreaks [37,38]. Higher chlorophyll-a concentration should be expected. For example, the magnitude of chlorophyll-a has reached ~60 mg·m^{-3} during the 2008 bloom event in the Gulf region as reported by Moradi and Kabiri [70]. Therefore, more *in situ* SDD measurements covering wider data range are required to improve the accuracy of the proposed model in this study. Other factors like temporal and spatial differences between satellite and *in situ* measurements, and sampling and measurement errors, also contributed to the uncertainties in the proposed algorithm to different extents.

4.3. Seasonal Variations of SDD in the Gulf

The new developed algorithm was used to analyze the seasonal variations of SDD in the Gulf. Seasonal SDD maps over the Gulf from 2002 to 2015 are shown in Figure 7. Stable features can be noticed. SDD values in the northern Gulf region close to Iraq are low, less than 1.5 m. This can be most likely attributed to the high loads of sediment from the Shatt al-Arab River that enters the Gulf along the Iraq-Iran borders. Similar characteristics can be found southwest of Iran, and northwest of the Strait of Hormuz also caused by river-borne sediments. At the meantime, bottom reflection should also be considered in interpreting those low SDD in shallow coastal waters where bottom reflection can increase satellite-derived K_d [59] although the contribution from bottom reflection may be low. SDD in the eastern area of Qatar and along the southwest coast of the UAE indicates consistently low values less than 4 m during the observation period. It should be noted that these areas are shallow and bottom reflection could contaminate satellite-derived K_d. These areas are sensitive marine ecosystems with coral reefs and sea grass. Some areas have been designated as Marine Protected Area (MPA), such as Marawah Marine Biosphere Reserve and Al Yasat MPA in the UAE. These MPAs are committed to conserve natural marine resources and ecosystems, and provide habitats for endemic wildlife. Time series of SDD averaged over the whole Gulf (bounded by 23.2°N–30.7°N and 47.3°E–56.5°E) for the period of 2002–2015 are shown in Figure 8. High SDD (10–11 m) were observed between late spring and early fall (April–September) while the low values (4–5 m) were recorded between late fall and early spring (October–March). In the hot summer season, the water column in the Gulf region is strongly stratified which prevents the nutrient-rich bottom water to be transported upward to the surface layer. Therefore, the nutrient supply for phytoplankton growth is depleted. In contrast, in the cold winter season, the water column mixes well by wind. Furthermore, the inflow of Indian Ocean surface waters (IOSW) through the Strait of Hormuz produces a cyclonic gyre in the Gulf region during winter [71]. Nutrient-rich bottom water is swirled up and supports phytoplankton growth. Upwelling has been identified as the main source of algal blooms in the Gulf [37]. On the other hand, strong winds prevail in winter, which causes sediment resuspension and thus decreases transparency. Inter-annual variations of SDD over the whole Gulf are not significant except for the years 2008–2013. SDD during 2008 and 2009, especially 2008, is remarkably lower than for other years. This is most likely related to the major algal bloom outbreak that started in late August 2008 and ended in late August 2009 [37]. The derived SDD in summer months between 2010 and 2013 was significantly larger than normal. Analysis indicated that transparency in May and June exhibited a monotonically increasing trend over the past 14 years. However, establishing a reason for this scene needs further measurements and investigations.

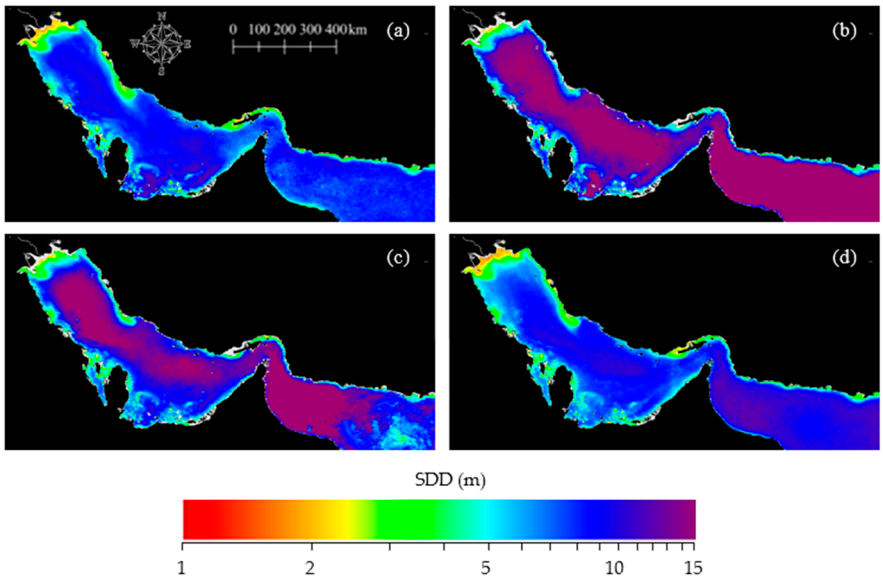

Figure 7. Seasonal SDD maps during the period of 2002–2015 over the Gulf calculated from Equation (9) using MODIS/Aqua data: (**a**) spring; (**b**) summer; (**c**) fall; (**d**) winter.

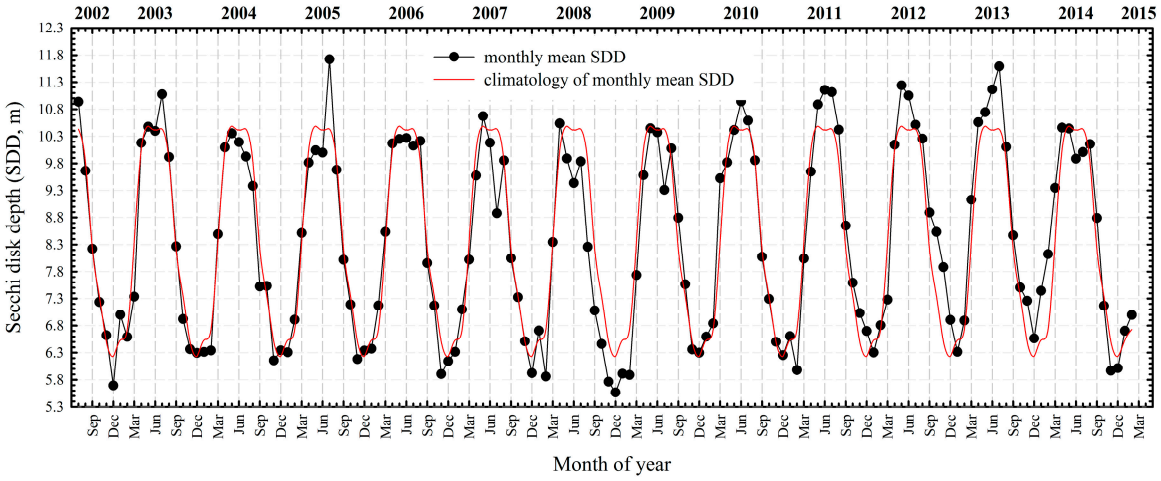

Figure 8. Time series of monthly mean SDD averaged over the entire Arabian Gulf between 2002 and 2015. The red line denotes climatology of monthly mean SDD.

5. Conclusions

Three models for estimating SDD over the Gulf region were tested using satellite measured K_d products, namely K_d_488_lee, K_d_490_morel and K_d_490_Mueller. Statistical results indicated that the model based on K_d_488_lee performed the best. Inter-annual variations of SDD from 2002 to 2014 over the whole Gulf region showed stable characteristics with low SDD <4 m in some coastal areas. This is attributed to the shallow bottom, high loads of river-borne sediments, coral reef, and benthic vegetation. Time series of monthly mean SDD over the whole Gulf region have shown typical subtropical trends with high values in summer and low values in winter. The inter-annual variations were found to be not significant except in 2008 and 2009 when an extensive, harmful algal bloom outbreak was recorded. Uncertainties of the proposed algorithm were mainly caused by atmospheric correction and shallow bottom reflection. Although more *in situ* measurements would be needed for better calibration and fair validation of the proposed algorithm, it still has the best performance when compared to the most widely used models in the literature.

Transparency is very essential to monitoring variations of water quality in local marine environment, to assess its effects on local marine ecosystems, and to examine the response of marine ecosystems to climate change and other human activities. The development and use of regional algorithms to estimate transparency, especially for optically complex coastal waters, are highly recommended. Having historical and real-time SDD maps with good accuracy over large temporal-spatial scales will be very useful for many marine-related researches.

Acknowledgments: The authors are very grateful to the Environmental Agency of Abu Dhabi for providing SDD data. We would like to thank group members in the Coastal and Environmental Remote Sensing and Modeling Laboratory at Masdar Institute of Science and Technology for collecting SDD data during filed campaigns. We also want to thank Bayanat and the UAE Navy for providing research vessels. We give our appreciations to the NASA Ocean Biology Processing Group (OBPG) for providing MODIS/Aqua data and the SeaDAS software package.

Author Contributions: Muna. R. Al Kaabi had the original idea and prepared the manuscript. Jun Zhao developed the algorithm, analyzed the data and designed the architecture of the manuscript. Hosni Ghedira contributed with ideas, discussions, and writing.

Conflicts of Interest: The authors declare no conflict of interest.

References

1. Dogliotti, A.I.; Ruddick, K.G.; Nechad, B.; Doxaran, D.; Knaeps, E. A single algorithm to retrieve turbidity from remotely-sensed data in all coastal and estuarine waters. *Remote Sens. Environ.* **2015**, *156*, 157–168. [CrossRef]
2. Kirk, J.T.O. Optical water quality—What does it mean and how should we measure it? *J. Water Pollut. Control Fed.* **1988**, *60*, 194–197.
3. Wilson, P.C. *Water Quality Notes: Water Clarity (Turbidity, Suspended Solids, and Color)*; University of Florida, Institute of Food and Agricultural Sciences (IFAS) and the Florida Cooperation Extension Service: Gainesville, FL, USA, 2013; pp. 1–8.
4. Liu, W.; Liu, Y.; Mannaerts, C.M.; Wu, G. Monitoring variation of water turbidity and related environmental factors in Poyang Lake national nature reserve, China. *Proc. SPIE* **2007**. [CrossRef]
5. IOCCG. *Remote Sensing of Ocean Color in Coastal, Other Optically-Complex, Waters*; IOCCG: Dartmouth, NS, Canada, 2000.
6. Forget, P.; Ouillon, S.; Lahet, F.; Broche, P. Inversion of reflectance spectra of nonchlorophyllous turbid coastal waters. *Remote Sens. Environ.* **1999**, *68*, 264–272. [CrossRef]
7. Prieur, L.; Sathyendranath, S. An optical classification of coastal and oceanic waters based on the specific spectral absorption curves of phytoplankton pigments, dissolved organic matter, and other particulate materials1. *Limnol. Oceanogr.* **1981**, *26*, 671–689. [CrossRef]
8. Megard, R.O.; Berman, T. Effects of algae on the secchi transparency of the southeastern mediterranean sea. *Limnol. Oceanogr.* **1989**, *34*, 1640–1655. [CrossRef]
9. Lewis, M.R.; Kuring, N.; Yentsch, C. Global patterns of ocean transparency: Implications for the new production of the open ocean. *J. Geophys. Res. Oceans* **1988**, *93*, 6847–6856. [CrossRef]
10. Garaba, S.; Voß, D.; Zielinski, O. Physical, bio-optical state and correlations in north-western european shelf seas. *Remote Sens.* **2014**, *6*, 5042. [CrossRef]
11. Garaba, S.P.; Friedrichs, A.; Voß, D.; Zielinski, O. Classifying natural waters with the forel-ule colour index system: Results, applications, correlations and crowdsourcing. *Int.J. Environ. Res. Public Health* **2015**, *12*, 16096–16109. [CrossRef] [PubMed]
12. Duntley, S.Q. Light in the sea. *J. Opt. Soc. Am.* **1963**, *53*, 214–233. [CrossRef]
13. Preisendorfer, R.W. *Hydrologic Optics*; National Technical Invormation Service: Springfield, VA, USA, 1976.
14. Zaneveld, J.R.; Pegau, W. Robust underwater visibility parameter. *Opt. Express* **2003**, *11*, 2997–3009. [CrossRef] [PubMed]
15. Aas, E.; Høkedal, J.; Sørensen, K. Secchi depth in the oslofjord-skagerrak area: Theory, experiments and relationships to other quantities. *Ocean Sci.* **2014**, *10*, 177–199. [CrossRef]
16. Holmes, R.W. The secchi disk in turbid coastal waters1. *Limnol. Oceanogr.* **1970**, *15*, 688–694. [CrossRef]
17. Lee, Z.; Shang, S.; Hu, C.; Du, K.; Weidemann, A.; Hou, W.; Lin, J.; Lin, G. Secchi disk depth: A new theory and mechanistic model for underwater visibility. *Remote Sens. Environ.* **2015**, *169*, 139–149. [CrossRef]

18. Koponen, S.; Pulliainen, J.; Kallio, K.; Vepsalainen, J.; Hallikainen, M. Use of Modis Data for Monitoring Turbidity in Finnish Lakes. In Proceedings of the IEEE 2001 International Geoscience and Remote Sensing Symposium, (IGARSS'01), Sydney, Australia, 9–13 July 2001; Volume 2185, pp. 2184–2186.
19. Chen, Z.; Muller-Karger, F.E.; Hu, C. Remote sensing of water clarity in tampa bay. *Remote Sens. Environ.* **2007**, *109*, 249–259. [CrossRef]
20. Moreno-Madrinan, M.J.; Al-Hamdan, M.Z.; Rickman, D.L.; Muller-Karger, F.E. Using the surface reflectance MODIS terra product to estimate turbidity in Tampa Bay, Florida. *Remote Sens.* **2010**, *2*, 2713–2728. [CrossRef]
21. Wang, M.; Nim, C.J.; Son, S.; Shi, W. Characterization of turbidity in florida's lake okeechobee and caloosahatchee and st. Lucie estuaries using MODIS-Aqua measurements. *Water Res.* **2012**, *46*, 5410–5422. [CrossRef] [PubMed]
22. Nehorai, R.; Lensky, I.M.; Hochman, L.; Gertman, I.; Brenner, S.; Muskin, A.; Lensky, N.G. Satellite observations of turbidity in the dead sea. *J. Geophys. Res. Oceans* **2013**, *118*, 3146–3160. [CrossRef]
23. Al-Saadi, H.; Saad, M.; Hadi, R.; Hussain, N. Further investigations on some environmental characteristics of north-west arab gulf. *Proc. Indian Natl. Sci. Acad.* **1977**, *43*, 183–192.
24. Alsahli, M.M.M.; Price, K.P.; Buddemeier, R.; Fautin, D.G.; Egbert, S. Modeling kuwait seawater clarity: A spatial-temporal study using remote sensing and gis. *Appl. Remote Sens. J.* **2012**, *2*, 17–33.
25. Al Kaabi, M.R.; Jun, Z.; Charron, C.; Gherboudj, I.; Lazzarini, M.; Ghedira, H. Developing Satellite-Based Tool for Water Turbidity Mapping in the Arabian Gulf: Abu Dhabi Case Study. In Proceedings of the 2013 Oceans—San Diego, San Diego, CA, USA, 23–27 September 2013; pp. 1–4.
26. Chen, Z.; Hu, C.; Muller-Karger, F. Monitoring turbidity in tampa bay using MODIS/Aqua 250-m imagery. *Remote Sens. Environ.* **2007**, *109*, 207–220. [CrossRef]
27. Lee, Z.-P.; Darecki, M.; Carder, K.L.; Davis, C.O.; Stramski, D.; Rhea, W.J. Diffuse attenuation coefficient of downwelling irradiance: An evaluation of remote sensing methods. *J. Geophys. Res. Oceans* **2005**, *110*. [CrossRef]
28. Zhao, J.; Barnes, B.; Melo, N.; English, D.; Lapointe, B.; Muller-Karger, F.; Schaeffer, B.; Hu, C. Assessment of satellite-derived diffuse attenuation coefficients and euphotic depths in south florida coastal waters. *Remote Sens. Environ.* **2013**, *131*, 38–50. [CrossRef]
29. Michael Reynolds, R. Physical oceanography of the gulf, strait of Hormuz, and the gulf of Oman—Results from the Mt Mitchell expedition. *Mar. Pollut. Bull.* **1993**, *27*, 35–59. [CrossRef]
30. Al Shehhi, M.R.; Gherboudj, I.; Ghedira, H. An overview of historical harmful algae blooms outbreaks in the arabian seas. *Mar. Pollut. Bull.* **2014**, *86*, 314–324. [CrossRef] [PubMed]
31. Johns, W.E.; Jacobs, G.A.; Kindle, J.C.; Murray, S.P.; Carron, M. *Arabian Marginal Seas and Gulfs: Report of a Workshop Held at Stennis Space Center, Mississipi*; University of Miami RSMAS: Miami, FL, USA, 1999.
32. Allan, T.D. The marine environment. *Int. J. Remote Sens.* **1992**, *13*, 1261–1276. [CrossRef]
33. Subba Rao, D.V.; Al-Yamani, F.; Nageswara Rao, C.V. Eolian dust affects phytoplankton in the waters off kuwait, the arabian gulf. *Naturwissenschaften* **1999**, *86*, 525–529. [CrossRef] [PubMed]
34. Mezhoud, N.; Temimi, M.; Zhao, J.; Al Shehhi, M.R.; Ghedira, H. Analysis of the spatio-temporal variability of seawater quality in the southeastern arabian gulf. *Mar. Pollut. Bull.* **2016**, *106*, 127–138. [CrossRef] [PubMed]
35. Mezher, T.; Fath, H.; Abbas, Z.; Khaled, A. Techno-economic assessment and environmental impacts of desalination technologies. *Desalination* **2011**, *266*, 263–273. [CrossRef]
36. Richlen, M.L.; Morton, S.L.; Jamali, E.A.; Rajan, A.; Anderson, D.M. The catastrophic 2008–2009 red tide in the arabian gulf region, with observations on the identification and phylogeny of the fish-killing dinoflagellate cochlodinium polykrikoides. *Harmful Algae* **2010**, *9*, 163–172. [CrossRef]
37. Zhao, J.; Ghedira, H. Monitoring red tide with satellite imagery and numerical models: A case study in the arabian gulf. *Mar. Pollut. Bull.* **2014**, *79*, 305–313. [CrossRef] [PubMed]
38. Zhao, J.; Temimi, M.; Ghedira, H. Characterization of harmful algal blooms (habs) in the arabian gulf and the sea of oman using meris fluorescence data. *ISPRS J. Photogramm. Remote Sens.* **2015**, *101*, 125–136. [CrossRef]
39. Essa, S.; Harahsheh, H.; Shiobara, M.; Nishidai, T. Chapter 3 operational remote sensing for the detection and monitoring of oil pollution in the arabian gulf: Case studies from the United Arab Emirates. In *Developments in Earth and Environmental Sciences*; Al-Azab, M., El-Shorbagy, W., Eds.; Elsevier: Amsterdam, The Netherlands, 2005; Volume 3, pp. 31–48.

40. Zhao, J.; Temimi, M.; Ghedira, H.; Hu, C. Exploring the potential of optical remote sensing for oil spill detection in shallow coastal waters-a case study in the arabian gulf. *Opt. Express* **2014**, *22*, 13755–13772. [CrossRef] [PubMed]
41. Mueller, J.L.; MOrel, A.; Frouin, R.; Davis, C.; Arnone, R.; Carder, K.L.; Lee, Z.P.; Steward, R.G.; Hooker, S.B.; Holben, B.; *et al. Ocean Optics Protocols for Satellite Ocean Color Sensor Validation, Revision 4, Volume III: Radiometric Measurements and Data Analysis Protocols*; NASA, Goddard Space Flight Center: Greenbelt, MD, USA, 2003.
42. Zhao, J.; Temimi, M.; Kitbi, S.A.; Mezhoud, N. Monitoring habs in the shallow Arabian Gulf using a qualitative satellite-based index. *Int. J. Remote Sens.* **2016**, *37*, 1937–1954. [CrossRef]
43. Bracchini, L.; Dattilo, A.M.; Hull, V.; Loiselle, S.A.; Tognazzi, A.; Rossi, C. Modelling upwelling irradiance using Secchi disk depth in lake ecosystems. *J. Limnol.* **2009**, *68*. [CrossRef]
44. Tyler, J.E. The secchi disc. *Limnol. Oceanogr.* **1968**, *13*, 1–6. [CrossRef]
45. Mueller, J.L. *Seawifs Algorithm for the Diffuse Attenuation Coefficient, k(490), Using Water-Leaving Radiances at 490 and 555 nm*; NASA Goddard Space Flight Cent.: Greenbelt, MD, USA, 2000; pp. 24–27.
46. Morel, A. Optical modeling of the upper ocean in relation to its biogenous matter content (case I waters). *J. Geophys. Res. Oceans* **1988**, *93*, 10749–10768. [CrossRef]
47. Morel, A.; Maritorena, S. Bio-optical properties of oceanic waters: A reappraisal. *J. Geophys. Res. Oceans* **2001**, *106*, 7163–7180. [CrossRef]
48. Bailey, S.W.; Franz, B.A.; Werdell, P.J. Estimation of near-infrared water-leaving reflectance for satellite ocean color data processing. *Opt. Express* **2010**, *18*, 7521–7527. [CrossRef] [PubMed]
49. Goyens, C.; Jamet, C.; Schroeder, T. Evaluation of four atmospheric correction algorithms for MODIS-Aqua images over contrasted coastal waters. *Remote Sens. Environ.* **2013**, *131*, 63–75. [CrossRef]
50. Bailey, S.W.; Werdell, P.J. A multi-sensor approach for the on-orbit validation of ocean color satellite data products. *Remote Sens. Environ.* **2006**, *102*, 12–23. [CrossRef]
51. Yao, F.; Johns, W.E. A HYCOM modeling study of the Persian Gulf: 1. Model configurations and surface circulation. *J. Geophys. Res. Oceans* **2010**, *115*. [CrossRef]
52. Wang, M.; Shi, W. The NIR-SWIR combined atmospheric correction approach for MODIS ocean color data processing. *Opt. Express* **2007**, *15*, 15722–15733. [CrossRef] [PubMed]
53. Nezlin, N.P.; Polikarpov, I.G.; Al-Yamani, F.Y.; Subba Rao, D.V.; Ignatov, A.M. Satellite monitoring of climatic factors regulating phytoplankton variability in the Arabian (Persian) Gulf. *J. Mar. Syst.* **2010**, *82*, 47–60. [CrossRef]
54. Pierson, D.C.; Kratzer, S.; Strömbeck, N.; Håkansson, B. Relationship between the attenuation of downwelling irradiance at 490 nm with the attenuation of PAR (400 nm–700 nm) in the Baltic Sea. *Remote Sens. Environ.* **2008**, *112*, 668–680. [CrossRef]
55. Suresh, T.; Naik, P.; Bandishte, M.; Desa, E.; Mascaranahas, A.; Matondkar, S.G.P. Secchi depth analysis using bio-optical parameters measured in the Arabian Sea. *Proc. SPIE* **2006**, *6406*. [CrossRef]
56. Stramska, M.; Stramski, D.; Hapter, R.; Kaczmarek, S.; Stoń, J. Bio-optical relationships and ocean color algorithms for the north polar region of the Atlantic. *J. Geophys. Res. Oceans* **2003**, *108*. [CrossRef]
57. Yuanzhi, Z.; Hui, L.; Chuqun, C.; Liding, C.; Bing, Z.; Anatoly, A.G. Estimation of chlorophyll-a concentration in estuarine waters: Case study of the Pearl River Estuary, South China Sea. *Environ. Res. Lett.* **2011**, *6*, 024016.
58. Hongtao, D.; Ronghua, M.; Yuanzhi, Z.; Steven Arthur, L.; Jingping, X.; Chenlu, Z.; Lin, Z.; Linlin, S. A new three-band algorithm for estimating chlorophyll concentrations in turbid inland lakes. *Environ. Res. Lett.* **2010**, *5*, 044009. [CrossRef]
59. Barnes, B.B.; Hu, C.; Schaeffer, B.A.; Lee, Z.; Palandro, D.A.; Lehrter, J.C. MODIS-derived spatiotemporal water clarity patterns in optically shallow florida keys waters: A new approach to remove bottom contamination. *Remote Sens. Environ.* **2013**, *134*, 377–391. [CrossRef]
60. Cannizzaro, J.P.; Carder, K.L. Estimating chlorophyll a concentrations from remote-sensing reflectance in optically shallow waters. *Remote Sens. Environ.* **2006**, *101*, 13–24. [CrossRef]
61. Wang, M.; Son, S.; Shi, W. Evaluation of MODIS SWIR and NIR-SWIR atmospheric correction algorithms using seabass data. *Remote Sens. Environ.* **2009**, *113*, 635–644. [CrossRef]
62. Menghua, W.; SeungHyun, S.; Yunlin, Z.; Wei, S. Remote sensing of water optical property for China's inland Lake Taihu using the SWIR atmospheric correction with 1640 and 2130 nm bands. *IEEE J. Sel. Top. Appl. Earth Obs. Remote Sens.* **2013**, *6*, 2505–2516.

63. Chen, S.; Zhang, T.; Hu, L. Evaluation of the NIR-SWIR atmospheric correction algorithm for MODIS-Aqua over the Eastern China Seas. *Int. J. Remote Sens.* **2014**, *35*, 4239–4251. [CrossRef]
64. Antón, M.; Valenzuela, A.; Román, R.; Lyamani, H.; Krotkov, N.; Arola, A.; Olmo, F.J.; Alados-Arboledas, L. Influence of desert dust intrusions on ground-based and satellite-derived ultraviolet irradiance in southeastern Spain. *J. Geophys. Res. Atmos.* **2012**, *117*. [CrossRef]
65. Fukushima, H.; Toratani, M.; Yamamiya, S.; Mitomi, Y. Atmospheric correction algorithms for ADEOS/OCTS ocean colar data: Performance comparison based on ship and buoy measurements. *Adv. Space Res.* **2000**, *25*, 1015–1024. [CrossRef]
66. Gordon, H.R. Atmospheric correction of ocean color imagery in the earth observing system era. *J. Geophys. Res. Atmos.* **1997**, *102*, 17081–17106. [CrossRef]
67. Carder, K.L.; Gregg, W.W.; Costello, D.K.; Haddad, K.; Prospero, J.M. Determination of Saharan dust radiance and chlorophyll from CZCS imagery. *J. Geophys. Res. Atmos.* **1991**, *96*, 5369–5378. [CrossRef]
68. Doxaran, D.; Devred, E.; Babin, M. A 50% increase in the mass of terrestrial particles delivered by the Mackenzie River into the Beaufort Sea (Canadian Arctic Ocean) over the last 10 years. *Biogeosciences* **2015**, *12*, 3551–3565. [CrossRef]
69. Qiu, Z.; Zheng, L.; Zhou, Y.; Sun, D.; Wang, S.; Wu, W. Innovative GOCI algorithm to derive turbidity in highly turbid waters: A case study in the Zhejiang coastal area. *Opt. Express* **2015**, *23*, A1179–A1193. [CrossRef] [PubMed]
70. Moradi, M.; Kabiri, K. Red tide detection in the strait of Hormuz (east of the Persian Gulf) using MODIS fluorescence data. *Int. J. Remote Sens.* **2012**, *33*, 1015–1028. [CrossRef]
71. Al Azhar, M.; Temimi, M.; Zhao, J.; Ghedira, H. Modeling of circulation in the Arabian Gulf and the sea of oman: Skill assessment and seasonal thermohaline structure. *J. Geophys. Res. Oceans* **2016**, *121*, 1700–1720. [CrossRef]